Experimental investigation of the packing structure of multi-sized spheres with liquid addition

Zou, Yi; Xu, Junqi; Wu, Yongli; Zou, Ruiping; Yu, Aibing

DOI
10.1016/j.powtec.2025.121684

Publication date
2025

Document Version
Final published version

Published in
Powder Technology

Citation (APA)
Zou, Y., Xu, J., Wu, Y., Zou, R., & Yu, A. (2025). Experimental investigation of the packing structure of multi-sized spheres with liquid addition. *Powder Technology*, *468*, Article 121684. https://doi.org/10.1016/j.powtec.2025.121684

Powder Technology 468 (2026) 121684

Contents lists available at ScienceDirect

Powder Technology

journal homepage: www.journals.elsevier.com/powder-technology

Experimental investigation of the packing structure of multi-sized spheres with liquid addition

Yi Zou [a], Junqi Xu [c], Yongli Wu [d,*], Ruiping Zou [e,*], Aibing Yu [b]

[a] ARC Research Hub for Smart Process Design and Control, Department of Chemical and Biological Engineering, Monash University, Clayton, Australia
[b] Southeast University-Monash University Joint Research Institute, Southeast University, Suzhou, China
[c] School of Materials Science and Engineering, The University of New South Wales, Sydney, Australia
[d] Faculty of Civil Engineering & Geosciences, Delft University of Technology, the Netherlands
[e] JITRI Institute for Process Modelling and Optimization, Suzhou, China

HIGHLIGHTS

- Experiments reveal the structure of wet particles with varying sizes.
- Packing structures show characteristics like agglomerates, clusters, and pores.
- Findings enable quantitative analysis of loosely packed multi-sized particles.
- Results aid in evaluating simulations of capillary/fluid forces in wet particles.

GRAPHICAL ABSTRACT

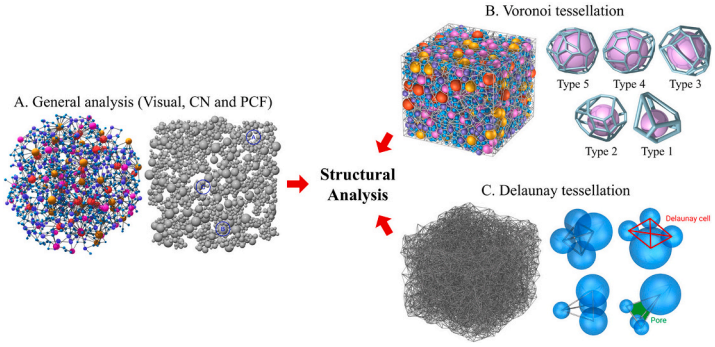

ARTICLE INFO

Keywords:
Wet particle packing
Packing structure
Coordination number
Pair correlation function
Voronoi tessellation
Delaunay tessellation

ABSTRACT

The packing of multi-sized wet spheres is highly intricate, shaped by the interplay of interparticle forces induced by the presence of liquid. This study presents a comprehensive and quantitative analysis of the microscopic particle arrangement within a multi-sized wet sphere packing. To achieve this, a multi-sized wet sphere packing is obtained experimentally and is then characterized by various analytical techniques, in terms of coordination number (CN), pair correlation function (PCF), topological and metric properties of the Voronoi-Delaunay tessellation. Through CN and PCF analysis, distinctive packing features such as agglomerates and particle chains are identified and characterized. Furthermore, the application of the Voronoi and Delaunay tessellation techniques uncovers the existence of heterogeneous clusters of particles in contact and non-contact states. These tessellation methods also shed light on the distorted pore structure that emerges within the packing. The insights gained from this study may serve to enhance the assessment and development of innovative simulation methods where capillary and liquid-related forces acting on wet particles with a size distribution are considered.

* Corresponding authors.
E-mail addresses: y.wu-7@tudelft.nl (Y. Wu), ruiping.zou@simpas.cn (R. Zou).

https://doi.org/10.1016/j.powtec.2025.121684
Received 15 February 2025; Received in revised form 19 August 2025; Accepted 20 September 2025
Available online 26 September 2025

1. Introduction

The packing of multi-sized particles is a crucial operation in various industries including mineral, materials, pharmaceutical, and chemical sectors [1]. The packing structure plays a pivotal role in determining structural properties such as conductivity and permeability, which directly impact product quality and process performance [2,3]. Research in particle packing primarily involves characterizing microscopic structures and quantifying the relationship between particle size and structural properties, challenges that are difficult to address with theoretical models alone. To overcome these challenges, both experimental [4–6] and numerical approaches [7–9] have been widely adopted. Experimental methods, such as optical microscopy, enable direct observation of particle packing structures. On the other hand, numerical simulations, particularly through the discrete element method (DEM) in recent years [10], provide additional insights and serve as an effective alternative for studying the structural dynamics of particle packings.

To comprehend the behavior, properties, and performance of particulate systems, it is necessary to quantify their microstructures. Over the years, several characterization methods have been proposed, including the coordination number (CN), pair correlation function (PCF), topological and metric properties of the Voronoi-Delaunay tessellation. CN, which represents the count of particles in close proximity to a specific particle, is often used as the first microscopic parameter for understanding the behavior and properties of particulate systems. It plays a significant role in analyzing the mechanical, thermal, and transport properties of such systems. Consequently, the coordination number has been extensively explored through experimental studies [11–18], analytical modelling [19–22], and numerical simulations [23–32]. This has also been applied to its parallel concept, i.e. PCF, in the literature.

The packing structure can also be quantified in terms of metric and topological properties using the so-called Voronoi-Delaunay tessellation [33–36]. The Voronoi tessellation provides more information about the spatial arrangements of particles compared to the radial distribution function or coordination number. It is valuable for quantifying properties related to particle connectivity, such as effective thermal conductivity. On the other hand, the Delaunay tessellation is particularly useful for investigating properties related to pore connectivity and pore-scale transport phenomena.

In contrast to non-cohesive particulate systems, cohesive particle packing involves multiple interparticle forces in addition to the gravity. These forces include the so-called van der Waals forces for fine particles [37–42] and cohesive forces associated for wet particles due to the formation of liquid bridges [43–47]. The presence of these cohesive forces significantly alters the static and dynamic behavior of particles, making it a central focus for granular researchers over the years. Both experimental [48–53] and numerical [54–57] approaches have been used to investigate these phenomena. For example, Feng and Yu [48] examined the impact of liquid addition on the packing of mono-sized coarse spheres and identified particle size and surface tension as crucial factors in quantifying the relationship between porosity and liquid content. Similar findings were reported in the studies of Zou et al. [49,50] on binary and polydisperse wet particle systems. Yang et al. [9] used the Discrete Element Method (DEM) to investigate the effect of liquid addition on the packing of mono-sized spheres, explicitly considering the capillary forces and quantifying the relationship between porosity and capillary force. Xu [51,52] analyzed the packing structure of narrowly sized wet sphere packings in terms of coordination number, radial distribution function, Voronoi tessellation, and Delaunay tessellation. Their analysis identified features such as large pores, aggregated particles, and chain-connected particles within the packing considered. Other researchers [58–60] have also contributed to the understanding of these phenomena using different approaches. However, most of these studies on wet particle packings are primarily focused on mono-sized particles and the effects of interparticle forces and liquid properties. Few studies have been given to the packing of multi-sized wet particles. Consequently, there is a scarcity of measurable and detailed structural information for multi-sized wet particles, making it challenging to provide an accurate microscopic description. While numerical methods have been used to obtain the loose packing structure of multi-sized cohesive particles, these approaches may not be widely applicable to wet particle systems. One of the difficulties here is the need for further validation through experimental investigation.

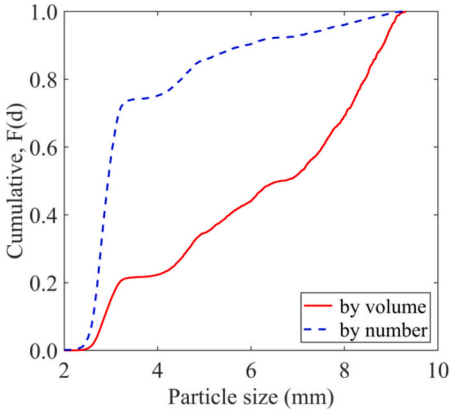

Fig. 1. Size distribution of the expanded polystyrene beads used.

Therefore, this study aims to experimentally achieve the packing of multi-sized wet spheres and quantitatively characterize its microscopic structures. It provides a comprehensive set of data about such a packing using various methods, including the coordination number, pair correlation function, and topological and metric properties of the Voronoi-Delaunay tessellation. Through these approaches, distinct packing features, such as agglomerates and pores, can also be identified and analyzed. This study offers better understanding of the complex microstructure of multi-sized wet packings and phenomena involving capillary and liquid forces in such systems.

2. Experimental method

The packing method used in this work is the same as that of our previous studies [51,52]. The experimental procedure for analyzing the packing of wet particles encompassed three primary stages: mixing, packing, and measurement. Initially, a predetermined quantity of liquid and particles was manually mixed to ensure even distribution of the liquid among the particles. Subsequently, this homogeneous particle-liquid mixture was gradually transferred into a pre-calibrated container using a funnel to create a packing. To determine the liquid content, the packing was first weighed after leveling off any excess particles. It was then weighed again following a drying process. The difference in weights, in conjunction with known densities of the particles and liquid, facilitated the calculation of liquid content. This was quantified as a volume ratio percentage between the liquid and the particles. Another key parameter measured was the dry-based packing density, which is the ratio of the volume of particles to the volume of the container. The dry-based porosity ε, by definition, equals one minus the packing density. It is important to note that in this experiment, tapping or compaction methods were deliberately omitted to specifically focus on the influence of liquid-induced forces.

In this study, expanded polystyrene beads were chosen for their low specific density of 0.136 g/cm^3, which aids in maximizing the impact of the capillary forces and enhancing measurement accuracy. The bead sizes were carefully selected to ensure a broad distribution, ranging from 1.86 to 9.46 mm, with an average diameter of 3.61 mm. Their cumulative size distribution by particle number and by particle volume are shown in Fig. 1, respectively. Optical examinations confirmed that these beads exhibit high sphericity, with a sphericity value exceeding 0.97,

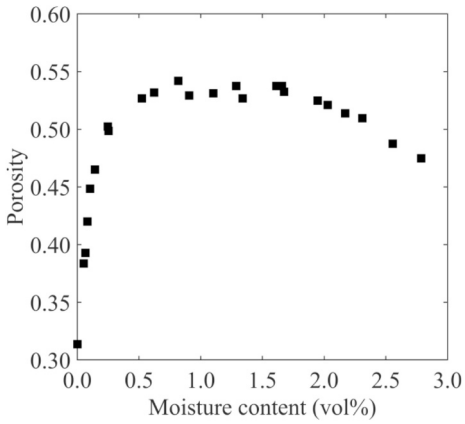

Fig. 2. The relationship between the porosity of the particle bed and liquid content.

indicating their near-perfect spherical shape. The experimental setup involved a container measuring 255 mm in diameter and 210 mm in height. After extensive testing, a dilute glue solution was selected as the liquid medium. Its specific density (0.995 g/cm^3), viscosity (0.0061 kg/(m·s)), and surface tension (0.0476 N/m). This particular solution was chosen because it could create a stable packing structure. The adhesive strength of the solution was sufficient to allow for the disassembly of the packing sample particle by particle, without altering the remaining structure. This characteristic was crucial for the accurate analysis of the packing behavior and the effects of capillary forces within the particle-liquid system.

The spatial coordinates of particles were precisely measured using a TM-500 digital microscope, complemented by a three-dimensional mechanical stage from Mitutoyo Corporation. This setup offered a high degree of accuracy in the measurements, with a precision of ±0.05 mm in the vertical direction and ± 0.01 mm in the horizontal direction. To mitigate the impact of the wall effect, which can skew results due to the influence of container boundaries, a specific sampling strategy was employed. A representative sample was extracted from the central region of the packing, ensuring a sufficient distance from the container's top, bottom, and walls. This distance was maintained at approximately five times the mean diameter of the particles, effectively reducing boundary-related anomalies in the data. The selected sample comprised a total of 10,697 particles. The coordinates and size of each individual particle within this sample were meticulously measured and recorded. This data was then digitized and stored in a computer system. The comprehensive collection of this spatial information enabled the accurate reconstruction of the packing structure in a virtual environment, facilitating in-depth analysis and study of the packing dynamics and properties.

3. Results and discussion

3.1. General characterization

Fig. 2 illustrates the correlation between dry-based porosity and liquid content in the study. As mentioned before, dry-based porosity ε is defined as one minus the packing density, where packing density is the ratio of the volume of particles to the volume of the container. The observed trend in the figure reveals an initial increase in porosity, reaching a peak, followed by a plateau, before decreasing as the liquid content further increases. This pattern is consistent with the previous research conducted on glass beads [50]. A notable observation from the study is that the maximum porosity recorded is 0.54, which is significantly higher than the 0.31 value found under dry conditions. The use of low-density particles was a deliberate choice in this study to achieve a packing with high porosity, thereby facilitating more precise structural measurements. Given these findings, the study focused on examining the packing structure at a liquid content of 2.1 %. At this specific liquid content, the overall porosity was observed to be 0.51. This particular point was chosen for detailed analysis as it represents a significant state within the observed trend, where the packing structure is influenced notably by the liquid content, allowing for meaningful insights into the interplay between liquid content and packing porosity.

Fig. 3(a) presents a comprehensive view of the entire measured block, while Fig. 3(b) offers a more focused depiction, revealing the internal structure and detailed arrangement of the spherical segment extracted from the central region of the measured block. In this latter figure, lines are utilized to denote the contact points between particles, providing a clear visual representation of particle interconnectivity. Notably, a visual inspection of these figures indicates that the particle distribution within the packing is not entirely uniform. Instead, it exhibits a propensity to form specific structural features, deviating from a

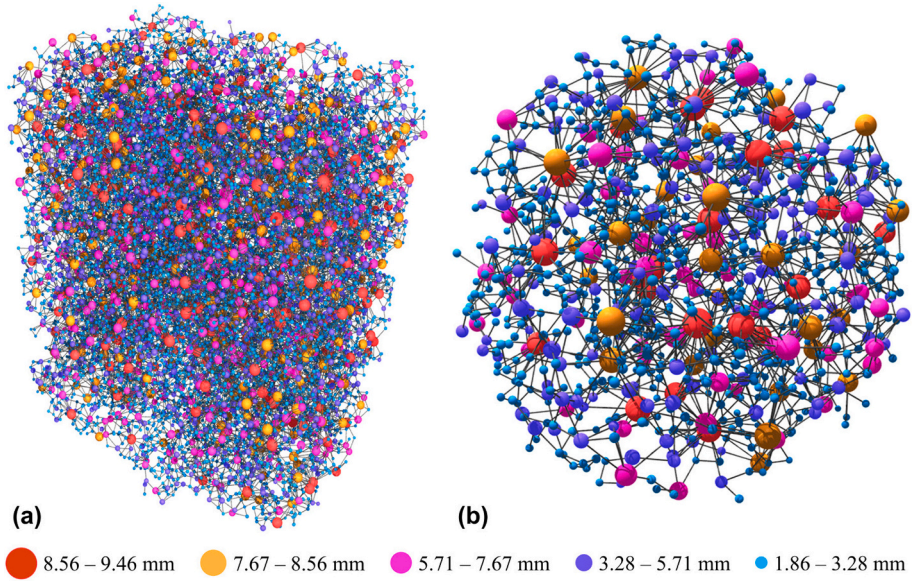

Fig. 3. (a) Overall view of the measured sample; (b) spherical sample taken from the center of the measured block, sticks represent the contacts between particles of different diameters shown.

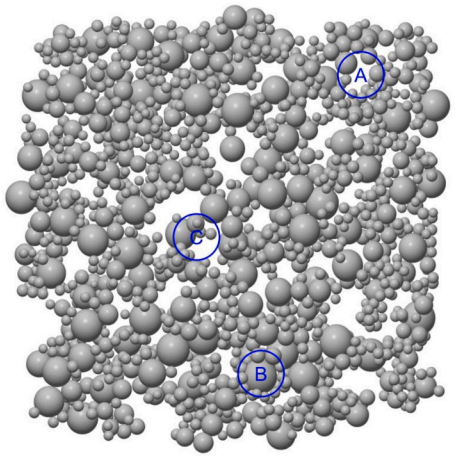

Fig. 4. Thin layer samples of 10 mm taken from the packing, where the red sticks represent the interparticle contacts, showing different structures such as sizable pores (A), particle cluster or agglomerate (B) and chain-like structure (C). (For interpretation of the references to colour in this figure legend, the reader is referred to the web version of this article.)

homogenous spread.

For a clearer view, Fig. 4 presents the interior view and intricate structure of three sample layers extracted from the analyzed packing, with red sticks denoting connections between particles. Upon examination, various packing characteristics emerge, such as sizable pores (A), particle agglomerates (B), and chain-like structures (C). The packing structure of multi-sized wet spheres is more complex compared to that of mono-sized wet spheres. Therefore, quantifying the structure is essential, as described in the following sub-sections using different methods of characterization.

3.2. Coordination number

The structure of a wet packing can generally be described by its CN. However, defining CN in this context necessitates the introduction of a separation distance since particles are not necessarily in direct contact. This distance represents the minimum gap between particles to determine whether they are in contact. Figs. 5(a) and 6(b) illustrate the effects of separation distance on the mean CN and CN distribution for various particle sizes, respectively. It can be observed that larger particles typically have higher mean CN values. As the chosen separation distance increases, the number of particle pairs considered to be in contact also rises for all particle sizes, with large particles being more affected due to their higher CN. The CN distribution peak for all particles shifts to higher values with increasing separation distance. The presence of larger particles contributes to a long tail at higher values in the distributions. For all sized particles, there is an overall mean CN which, corresponding to Fig. 5(a), increases with the critical distance as shown in Fig. 6.

In order to facilitate a more detailed analysis, in the following, particles are categorized into five types based on their volume. Table 1 presents the size range and mean size for each particle type. Different types of particles may contact with each other, giving the so called

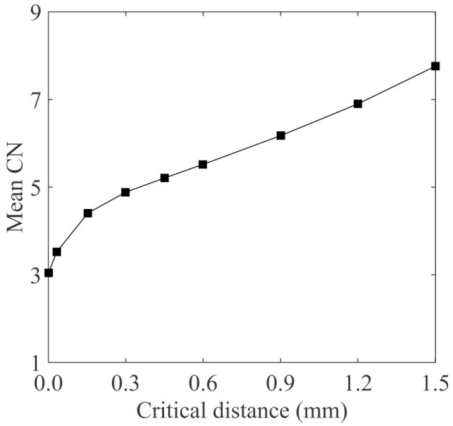

Fig. 6. Overall mean CN as a function of separation distance.

Table 1
Particle size ranges for each particle type.

Size (mm)	From	To	Mean	Volume fraction
Type 1	1.86	3.28	2.57	21.10 %
Type 2	3.28	5.71	4.50	20.68 %
Type 3	5.71	7.67	6.69	21.24 %
Type 4	7.67	8.56	8.12	20.88 %
Type 5	8.56	9.46	9.01	16.09 %

Table 2
Partial mean CN of each type of particles.

	Type 1	Type 2	Type 3	Type 4	Type 5
Type 1	1.79	0.70	0.41	0.30	0.28
Type 2	2.89	1.11	0.50	0.35	0.32
Type 3	5.08	1.50	0.55	0.36	0.35
Type 4	6.62	1.91	0.65	0.61	0.39
Type 5	8.19	2.21	0.82	0.51	0.28

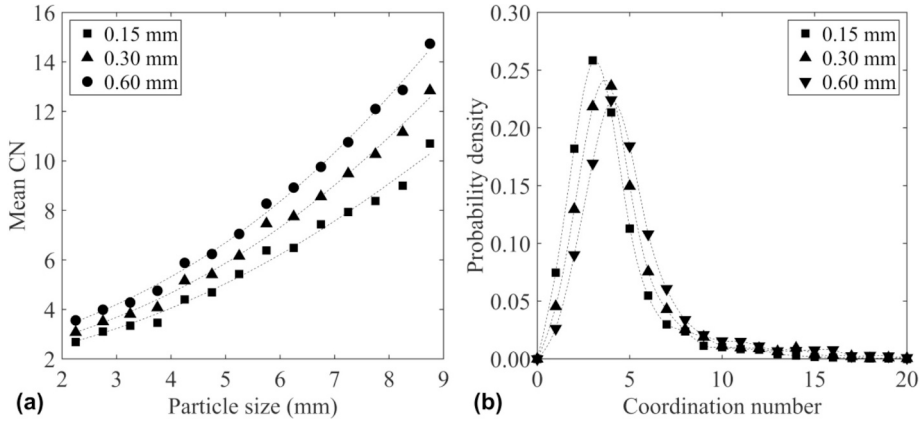

Fig. 5. (a) Mean CN of different particle size, and (b) CN frequency distribution for different separation distances.

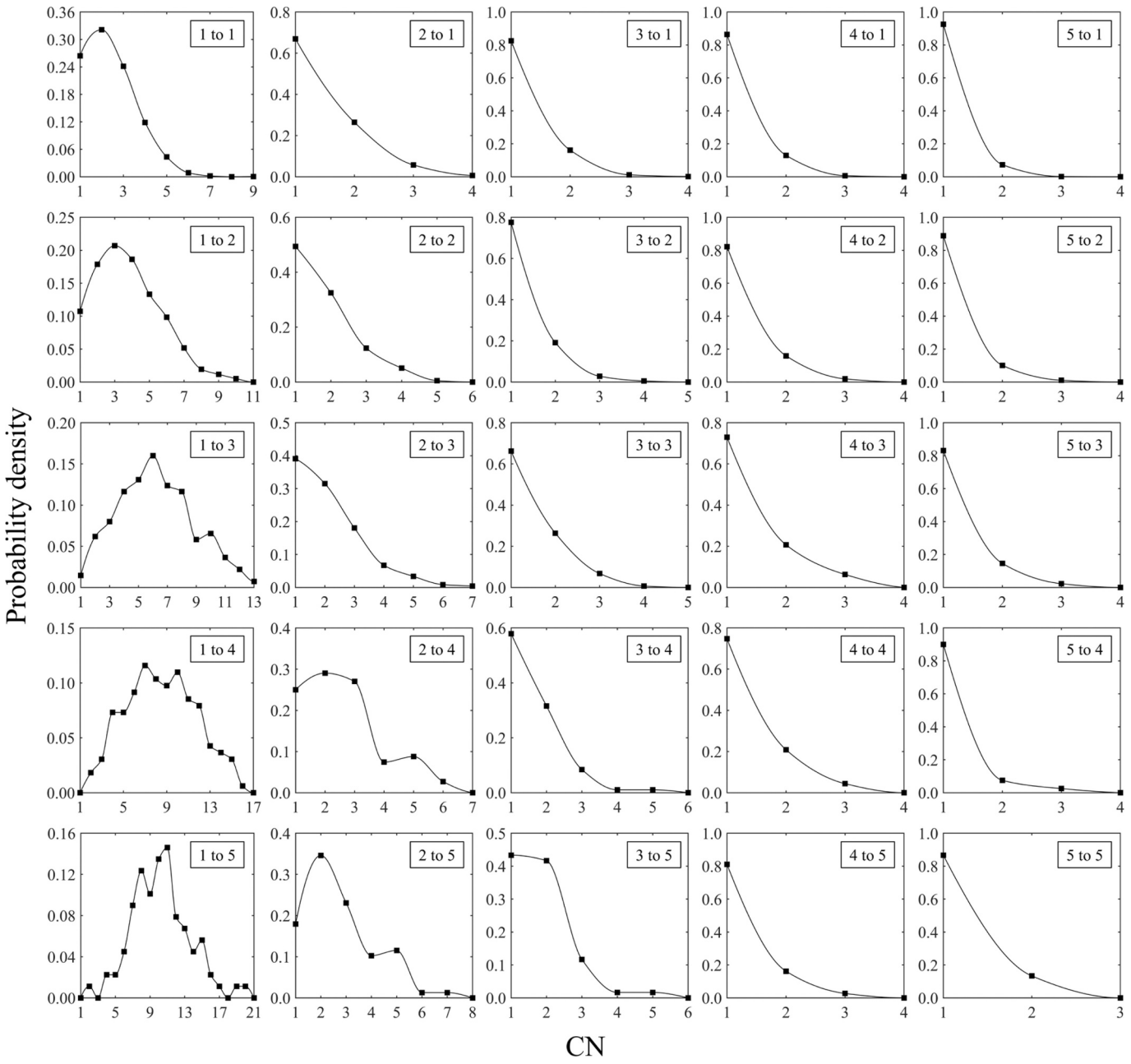

Fig. 7. Partial CN distributions of different types of contacts for 5 types of particles.

partial coordination numbers [1,16,17,19]. Table 2 then illustrates the partial mean CN associated with each type of contact. A notable pattern emerges in each row of Table 2: the values generally decrease from left to right. This indicates that particles are more likely to contact smaller particles than larger ones. A significant reduction in CNs is evident along the diagonal of the matrix, signifying a reduced tendency for particles of the same type to contact with each other as their size increases. This suggests that larger particles tend to be more dispersed within the packing. For smaller particle types, such as Types 1 and 2, the CNs typically increase when these particles interact with larger ones, as observed when moving rightward across a row. This trend implies that smaller particles are more likely to cluster around or interact more frequently with larger particles. Conversely, larger particles (Types 4 and 5) show higher CNs across all particle types, highlighting their central role in the interaction dynamics of the particle system. They may act as focal points or hubs in the formation of agglomerates, as seen in Fig. 4.

The distributions of partial CNs, as illustrated in Fig. 7, reveal distinct patterns for small and large size particles. For the five types of particles, there are different types of contacts, giving different partial CN. In this context, the partial CN of Type A to Type B represents the average number of Type B particles surrounding a Type A particle. For particles of smaller sizes, there is a notable tendency for them to frequently contact each other, often establishing multiple contacts with particles of the same type. In contrast, larger particles, particularly Types 4 and 5, predominantly contact smaller particles. This difference in contact patterns suggests that while smaller particles tend to form clusters with each other, larger particles are more dispersed within the system. Larger particles require a higher critical volume fraction to make contact with each other. Conversely, smaller particles can form a connected network at a lower volume fraction. The introduction of liquid and the resulting capillary forces significantly affect the system's dynamics. Smaller particles are more likely to adhere to larger particles rather than occupying the voids between them. These small particles also tend to

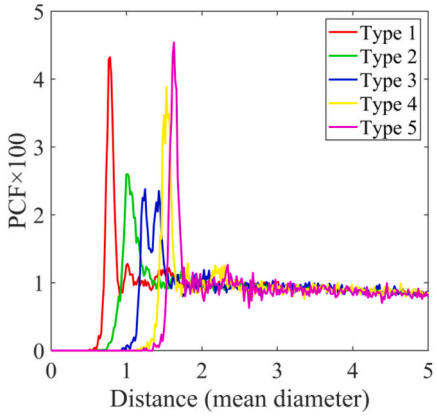

Fig. 8. PCF of different types of particles as a function of distance.

aggregate, forming larger clusters. The formation of these agglomerates, coupled with the capillary forces, contributes to the high porosity observed in the packing. Consequently, larger particles require an even higher critical volume fraction to bridge the gaps created by the small particles and the large voids. In the studied system, the volume fraction of large particles is insufficient to form a connected network. However, small particles demonstrate a high level of connectivity under the current conditions. For instance, over 50 % of Type 1 particles have a partial CN greater than one when interacting with particles of the same type (Type 1). These distributions well correspondnto the complex structure observed in Figs. 3 and 4.

In general, the CN results align well with those reported in the literature [17,61]. Geometrically, larger particles tend to have a higher mean partial CN due to their larger contact area, as illustrated in Fig. 5. Statistically, particles with a higher number fraction have a greater probability of forming contacts. Consequently, smaller particles, which have a high number fraction as shown in Fig. 1, significantly contribute to the CN of larger particles, particularly for interactions between Type 1 particles and Type 4 or Type 5 particles, as depicted in Fig. 7. This trend would not change between dry and wet particle mixtures.

3.3. Pair correlation function

The concept of PCF has been widely used to describe the structure of particle systems. PCF is to some degree related to CN, considering the pairing between particles. Here, the non-normalized PCF is defined as:

$$g_{i,j}(r) = \frac{N_{i,j}(r)}{4\pi r^2 \Delta r}\# \tag{1}$$

where $g_{i,j}(r)$ is the probability of finding a j-type particle center around an i-type particle in the distance between r and $r + \Delta r$. Δr is the calculation step. $N_{i,j}(r)$ is the average number of j-type particles around an i-type particle in the sphere shell between r and $r + \Delta r$ and expressed as:

$$N_{i,j}(r) = \frac{\sum_{i=1}^{N_i} n_j(r)}{N_i}\# \tag{2}$$

where N_i is the number of i-type particles calculated, and $n_j(r)$ is the number of j-type particles around an i-type particle in the sphere shell between r and $r + \Delta r$.

In the current system, for each type of particles, there is a mean PCF $g_1, g_2, \ldots g_5$, irrespective of the types of particles in pair. For each type of particle pair, there is also a partial PCF, $g_{11}, g_{12}, \ldots g_{55}$, respectively, representing the contributions of different types of pairs. Fig. 8 presents the partial PCFs of different particle types. The distance r is expressed in dimensionless mean diameter for all particles, done by dividing a particle size considered. As shown in the figure, for each particle type, the PCF exhibits strong peaks at the beginning of the curves, indicating the formation of agglomerates where Type 1 particles surround each particle type. The position of these peaks shifts to the right as particle size increases, reflecting the larger distances associated with larger particle sizes. Due to the higher ratio of capillary force to gravity for smaller particles, these particles are more likely to come into contact with others. This tendency leads to peak positions that approximately correspond to the sum of the mean radius of two particles: the radius of the given particle type and the mean radius of Type 1 particles.

The PCF between different types of particles is used to examine the detailed packing structure, as shown in Fig. 9. All partial PCFs exhibit a pronounced first peak, except for the Type 5-Type 5 partial PCF. Some partial PCFs also display a significant second peak, while others fluctuate after the first peak. These complex patterns arise from the intricate packing structure of wet, multi-sized particles. As noted earlier, the packing consists of various sizes of agglomerates and voids, with the agglomerates formed by particles of different sizes. For smaller particles, particularly Type 1 particles, there is a connected network, as discussed in the CN section. The small peaks at $r = 1.43$ (5.16 mm) likely result from three particles aligned or nearly aligned. This three-particle alignment may also contribute to the second peaks observed in Type 1-Type 3 partial PCF and Type 1-Type 4 partial PCF. In these cases, a larger particle (Type 3 or Type 4) typically occupies one end of the chain. The absence of a strong peak in the Type 5-Type 5 partial PCF suggests that large particles are well-separated by other particle types and voids.

The PCFs of multi-sized particle mixtures are much more complicated than mono-sized particles, as reported by Yang et al. [9]. Such complication is inherited for wet particle packing. However, as shown in Fig. 4, the present packing includes complicated packing structures, such as compact cluster same as dry packing, loose structure with big voids, and small one between, due to different connections between clusters, and loose structures. Hence, the PCF shows an even more complicated and anisotropic structure as discussed above.

3.4. Voronoi tessellation

The Voronoi tessellation method was employed on 4081 core particles within the observed wet packing, effectively eliminating the influence of peripheral particles, as depicted in Fig. 10. The right portion of the figure showcases a representative schematic of characteristic Voronoi cells corresponding to different particle categories. A comprehensive analysis of both topological and metric properties is performed using the so-called radical tessellation [35,62]. Topological attributes include the number of faces f and edges e for each polyhedron, while metric properties encompass the area A and perimeter L of individual polyhedron faces and the perimeter P, area S, volume V, and sphericity ψ of each Voronoi polyhedron.

The number of faces per polyhedron is a critical local structural property. Unlike CN, two particles are considered neighbors if they share a radical face, even if they are not in contact. This concept is especially relevant when examining a structural property that relies heavily on the connectivity among particles in a packed bed, e.g., the thermal conductivity or radiation of a particle bed [3,63]. Fig. 11(a) displays the distribution of the number of faces for Voronoi polyhedra for all particles, with Fig. 11(b) illustrating the relationship between the mean particle size and number of faces. As depicted, the relationship is nearly linear, with the number of polyhedral faces increasing with particle size. The distribution reveals a peak around 12, which is slightly lower than that of uniform wet or fine spheres [34,52]. This could result from the polyhedra of the large number of small particles. Additional minor peaks are present in the distribution's long tail, contributed by larger particles. Fig. 11(c) presents the partial distributions for various particle types. For small particles, in addition to the peak around 12, there is a short tail suggesting the presence of small agglomerates of different distorted shapes. In the case of large particles (e.g., Types 4 and 5), the

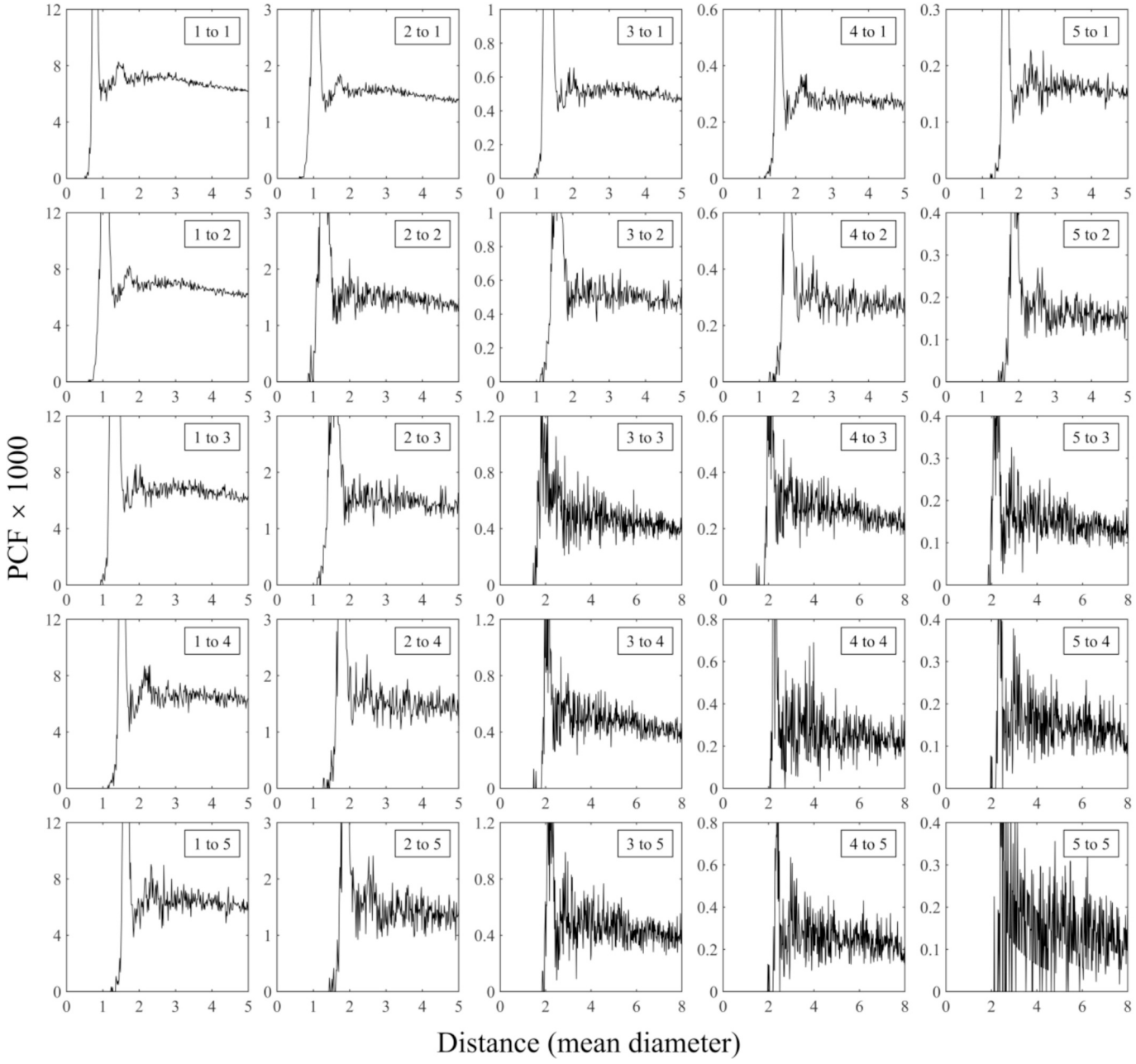

Fig. 9. Partial PCFs of different particle types.

distribution curves become less smooth, indicating that these particles are well-separated and surrounded by many smaller particles of different types.

Fig. 12 presents the results for the number of edges per polyhedron face. As can be observed from Fig. 12(a), the distribution of edge numbers for all particles peaks at around 5, and Fig. 12(b) demonstrates that the edge number marginally increases with particle diameter. Fig. 12(c) reveals that the distributions for different particle types exhibit a similar pattern; the distribution shifts slightly to the right as particle size increases. According to Yang et al. [34], the average edge number e and face number f for a Voronoi tessellation conform to $e = 6 - 12/f$ in a random packing, which suggests that the edge number changes far less significantly with increasing face number. Consequently, the most probable values for edge numbers are 4, 5, and 6, accounting for the peak in the distribution of edge numbers for particles of all sizes. These results are consistent with other multi-sized packing systems [35,36], indicating that the key feature of edge numbers may generally be valid for all multi-sized systems.

The metric properties of the radical polyhedra are also examined, including face-related attributes such as relative face perimeter L^* and face area A^*, displayed in Figs. 11 and 12, respectively. Here, relative property X^* is defined as: $X^* = X/\langle X \rangle$. Fig. 13(a) illustrates the distribution of the face perimeter for all particles, while the distributions of the face perimeter for different particle types are given in Fig. 11(c). The distribution indicates that as particle size increases, the likelihood of faces having infinitesimally small perimeters decreases, and the overall distribution shifts rightwards, suggesting an increase in the polyhedral face perimeters.

Concerning the distribution of the face area, Fig. 14(a) exhibits one major peak in the distributions. This peak emerges near zero due to the physical constraint dictating that a face must exceed a certain minimum value, as two proximate particles cannot overlap [34]. The partial distributions in Fig. 14(c) shift towards the right as particle size increases, indicating a general enlargement in the polyhedral face. This is also

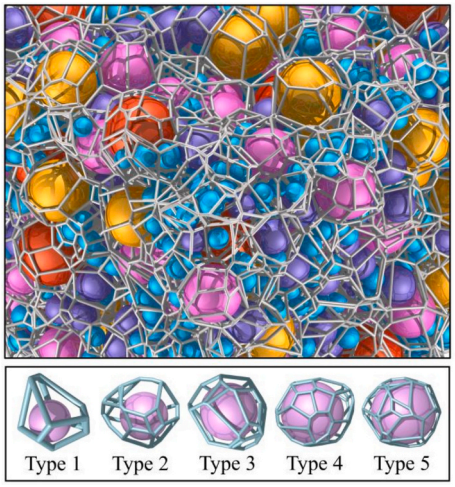

Fig. 10. Voronoi tessellation of the multi-sized wet particle packing (top) and the resulting typical Voronoi polyhedra for different types of particles (bottom).

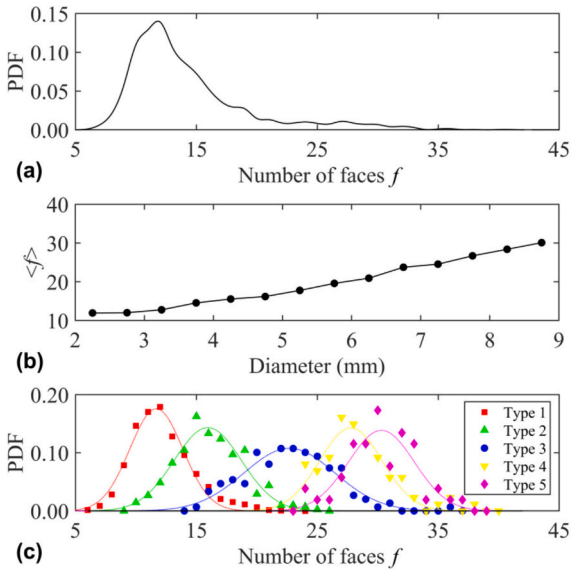

Fig. 11. (a) Distribution of the number of faces f for the Voronoi polyhedra for all particles; (b) relationship between the mean number of faces $\langle f \rangle$ and particle diameter; and (c) distribution of the number of faces f for the Voronoi polyhedra among different particle types.

depicted in terms of the relationship between the overall mean face perimeter/area and particle diameter in Figs. 13(b) and 14(b). The variation in the face perimeter and area with particle size can provide insights into the configuration of particle agglomerates. For large particles, the distribution of both the face perimeter and face area exhibits only a slight rightward shift. This indicates that a large particle is predominantly surrounded by small-size particles. In other words, large particles are typically located at the center of agglomerates.

Figs. 15, 16, and 17 show cell-related properties, including the relative cell perimeter P^*, surface area S^*, and volume of a Voronoi polyhedron V^*, respectively. These are the metric properties of the Voronoi tessellation. The overall distributions of these properties are depicted in Figs. 15(a), 16(a), and 17(a). Each distribution features a prominent peak associated with the Voronoi cells of small particles, followed by a long tail corresponding to the cells of larger particles. Figs. 15(b), 16(b), and 17(b) demonstrate that the average values of cell perimeter, surface area, and volume increase in proportion to particle size. This trend is further corroborated by the partial distributions for

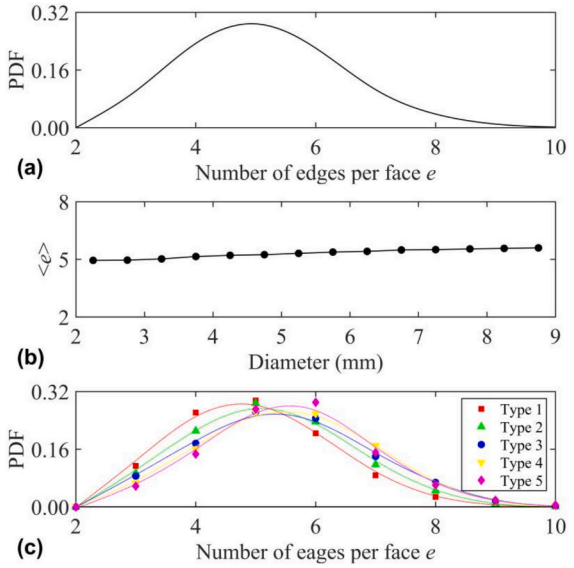

Fig. 12. (a) Distribution of the number of edges per face e for the Voronoi polyhedra for all particles; (b) relationship between the mean number of faces $\langle e \rangle$ and particle diameter; (c) distribution of the number of edges per face e for the Voronoi polyhedra among different particle types.

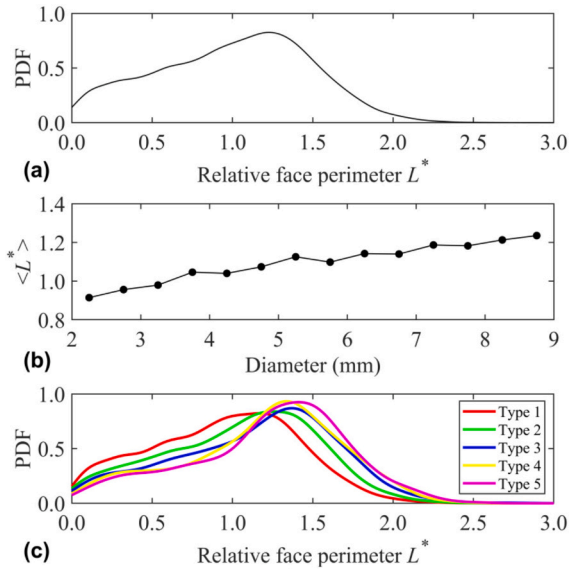

Fig. 13. (a) Distribution of the relative face perimeter L^* for the Voronoi polyhedra for all particles; (b) relationship between the mean relative perimeter $\langle L^* \rangle$ and particle diameter; (c) distribution of the relative face perimeter L^* for the Voronoi polyhedra among different particle types.

different particle types, as shown in Figs. 15(c), 16(c), and 17(c). These observations align with the geometric principle that a polyhedron must be adequately sized to encase a particle of a specific size. Consequently, the peaks in these distributions, which are organized in ascending order of their values, correspond to particle components ranging from small to large sizes.

The shape of the Voronoi polyhedra is also examined in terms of sphericity ψ, which is defined as the ratio of the surface area of a sphere to that of a polyhedron of the same volume [33]. A higher sphericity implies a more spherical polyhedron. Fig. 18(a) shows that the distribution of overall sphericity has a major peak near 0.8, which is lower than 0.87 for uniform wet particles [52] and 0.9 for uniform fine particles [34]. The presence of the capillary effect combined with fewer

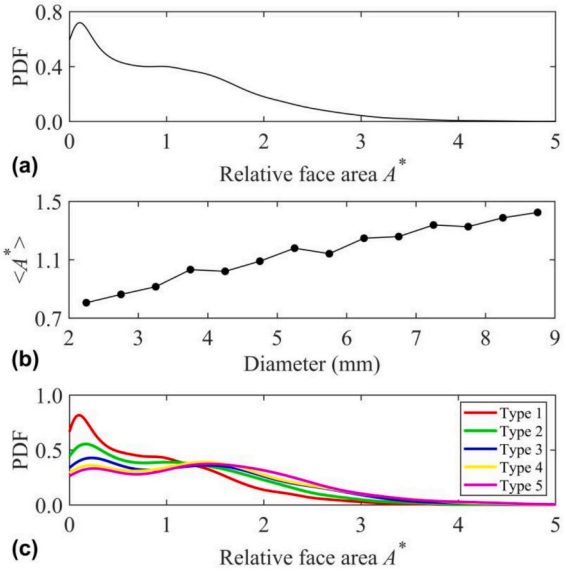

Fig. 14. (a) Distribution of the relative face area A^* for the Voronoi polyhedra for all particles; (b) relationship between the mean relative face area $< A^* >$ and particle diameter; (c) distribution of the relative face area A^* for the Voronoi polyhedra among different particle types.

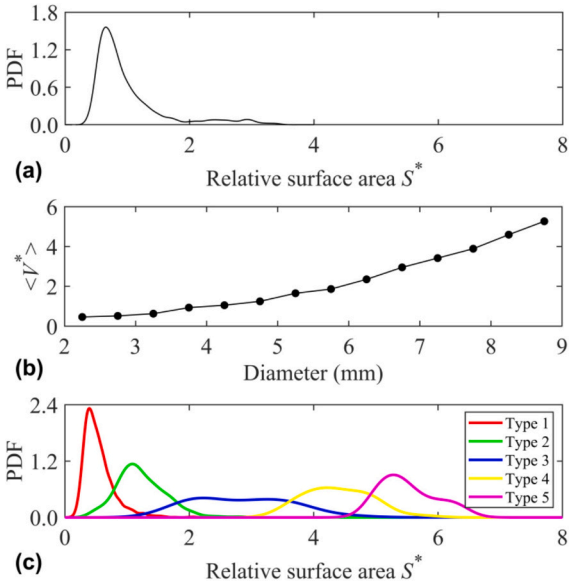

Fig. 16. (a) Distribution of the relative surface area S^* for the Voronoi polyhedra for all particles; (b) relationship between the mean relative surface area $< S^* >$ and particle diameter; (c) distribution of the relative surface area S^* for the Voronoi polyhedra among different particle types.

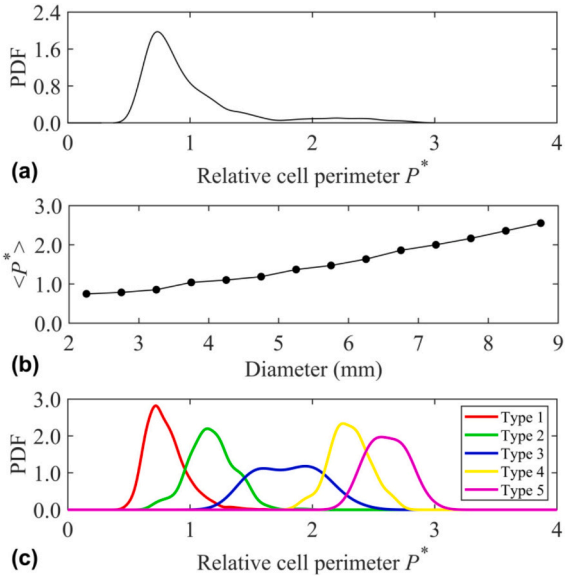

Fig. 15. (a) Distribution of the relative cell perimeter P^* for the Voronoi polyhedra for all particles; (b) relationship between the mean relative cell perimeter $<P^*>$ and particle diameter; (c) distribution of the relative cell perimeter P^* for the Voronoi polyhedra among different particle types.

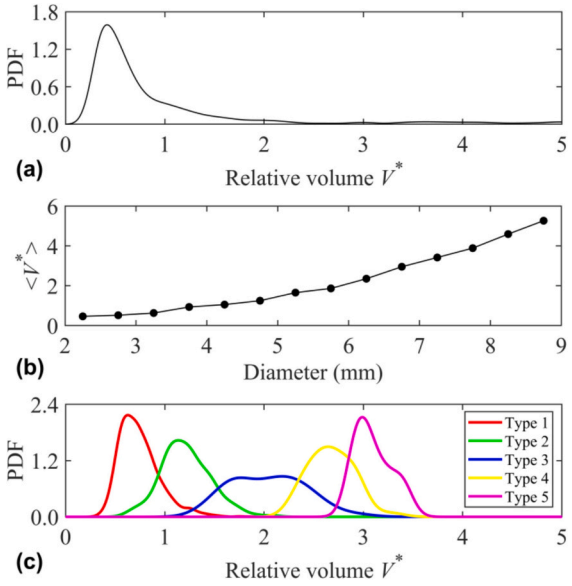

Fig. 17. (a) Distribution of the relative volume V^* for the Voronoi polyhedra for all particles; (b) relationship between the mean relative volume $< V^* >$ and particle diameter; and (c) distribution of the relative volume V^* for the Voronoi polyhedra among different particle types.

surrounding particles can result in structures with reduced sphericity. As shown in Fig. 18(b), the sphericity of the polyhedra increases as the particle size enlarges. The sphericity distributions for polyhedra of different particle types are given in Fig. 18(c). As observed, the distribution becomes taller and narrower as particle size increases, suggesting that the polyhedra of larger particles are not only more spherical but also exhibit less shape deviation compared to smaller particles. This typically occurs when a large particle is surrounded by numerous small particles, resulting in Voronoi polyhedra with small yet numerous faces enveloping the large particle. Within the packing, the influence of the capillary effect is more pronounced for smaller particles. Additionally, these smaller particles are surrounded by fewer neighbors, contributing to their decreased sphericity.

3.5. *Delaunay tessellation*

Delaunay tessellation and Voronoi tessellation are dual structures in computational geometry, closely related through their geometric and mathematical properties. Each vertex of the Voronoi diagram corresponds to a circumcenter of a Delaunay triangle; and each edge of the Voronoi diagram is perpendicular to and bisects an edge of the Delaunay triangulation. Delaunay tessellation is widely used to characterized the pore structure within particle packing [64,65].

The Delaunay cell encapsulates the structure of tetrahedra, each

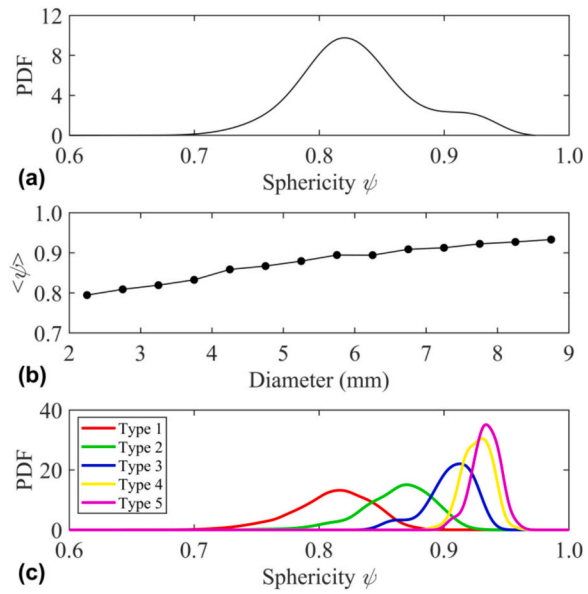

Fig. 18. (a) Distribution of the sphericity ψ for the Voronoi polyhedra for all particles; (b) relationship between the mean sphericity $<\psi>$ and particle diameter; (c) Distribution of the sphericity ψ for the Voronoi polyhedra among different particle types.

composed of four particles. The volume of a pore refers to the void space within a Delaunay cell, and its characteristics can be assessed based on its geometric properties, such as size and shape. The Delaunay tessellation was executed for the 4081 particles located at the center of the measured wet packing, as depicted in Fig. 19. In this study, we concentrate on the size and shape of the Delaunay cells and pores, as well as their correlation. Here, the size of Delaunay cells/pores, denoted as d^*, is characterized by their equivalent volume diameter, which is expressed as: $d^* = \sqrt[3]{6V/\pi}$, V is the volume of cell/pore. The shape is represented in terms of sphericity of each cell/pore, which is defined in a manner analogous to that used for Voronoi polyhedra.

Fig. 20(a) presents the size distribution of the Delaunay cells, indicating that the packing possesses a somewhat asymmetric distribution with a pronounced peak around 2.8 mm, approximating the mean size of type 1 particles. The relatively broad distribution suggests that the Delaunay cells are considerably distorted due to the size distribution of particles. Fig. 20(b) depicts the distribution of cell sphericity. The distribution for this packing has a strong peak at $\psi = 0.6$, accompanied by a long tail at lower sphericity values. Given that a regular tetrahedron has a sphericity of 0.67, this suggests that most of the cells are slightly distorted near-regular tetrahedra, presumably formed by many small particles of varying sizes. The long tail at lower sphericity represents distorted cells, aligning with the findings from Fig. 20(a).

According to the present approach, each Delaunay cell, as a tetrahedral subunit, can be characterized by two independent parameters: size and sphericity. The correlation between them is shown in Fig. 20(c). Although a basic trend that larger cells tend to have higher sphericity

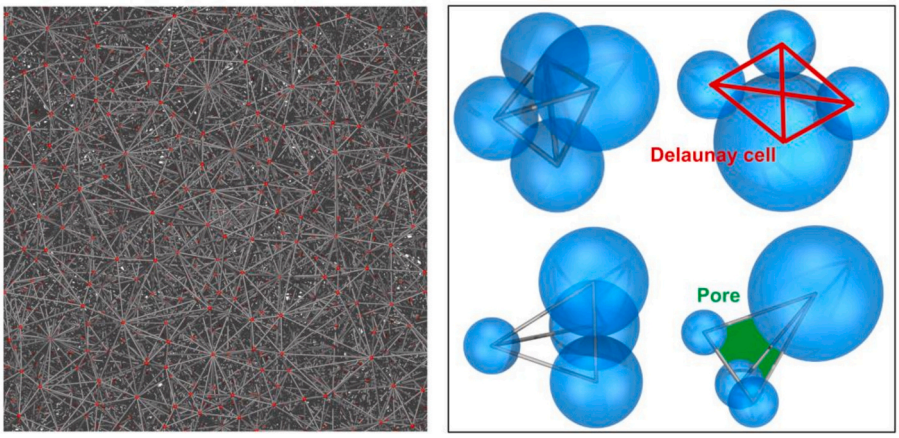

Fig. 19. Delaunay tessellation applied to the packing (left) and an illustration of the pore structure (right).

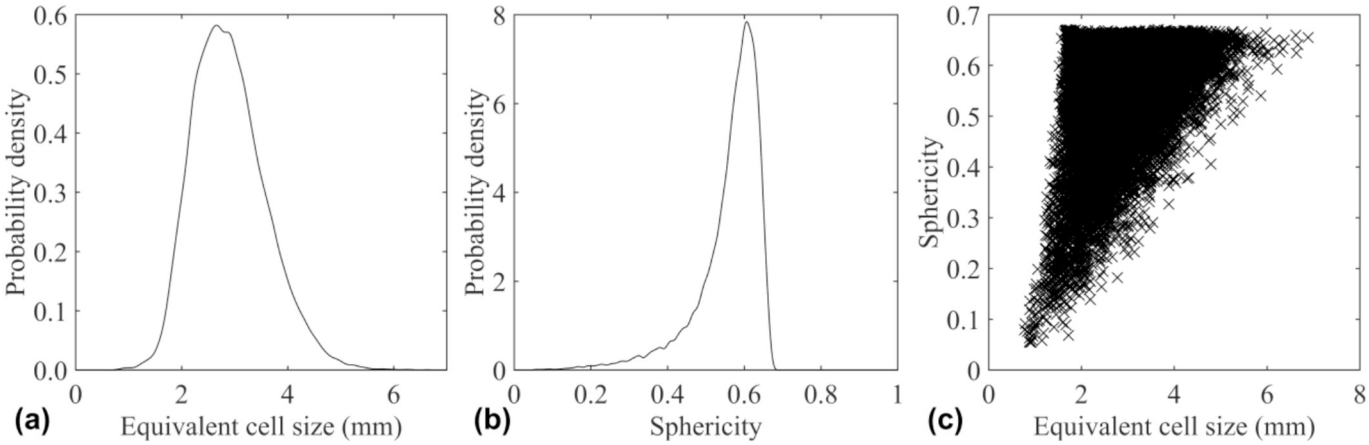

Fig. 20. (a) Distribution of Delaunay cell size d_c^*; (b) Distribution of cell sphericity ψ_c; (c) Correlation between Delaunay cell size and shape.

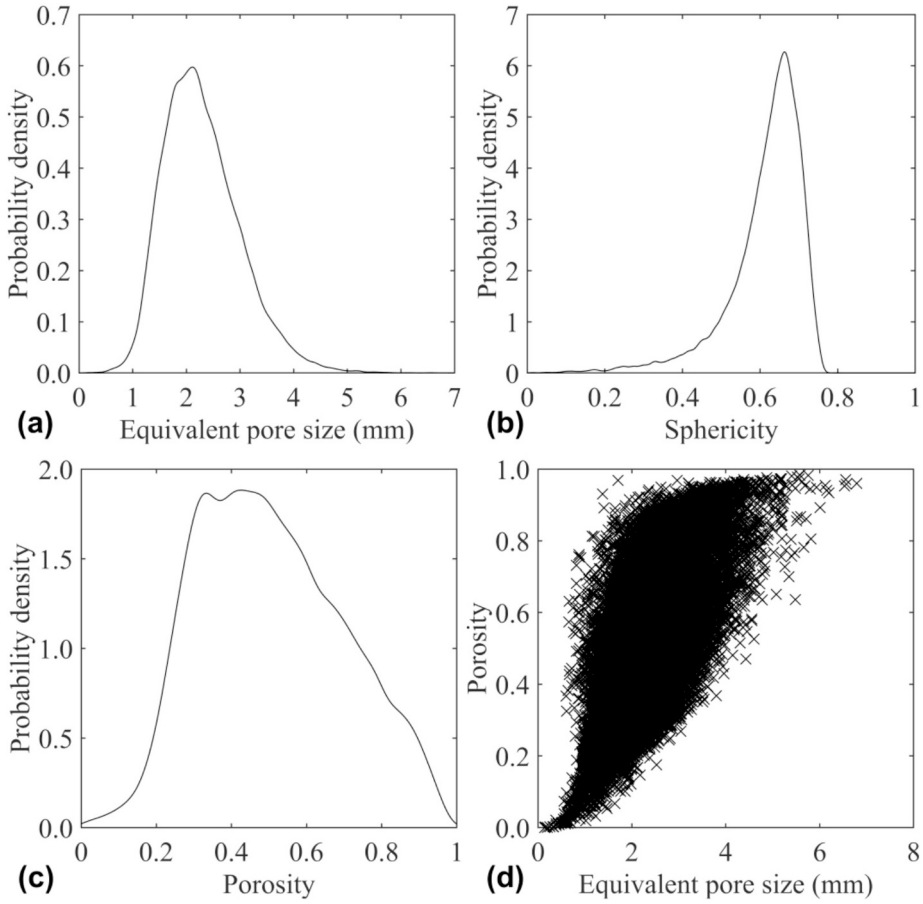

Fig. 21. Distribution of: (a) pore size d_p^*, (b) pore sphericity ψ_p and (c) pore porosity ε; (d) correlation between pore size and pore porosity.

can be observed, the correlation between cell size and cell sphericity is quite scattered. This is because in a wet multi-sized system, the cohesive force plays an important role, more Delaunay cells are formed by "untouching" particles and become more irregular.

In a Delaunay cell, the region not occupied by particles is termed as 'pore space.' The distribution of both pore size and sphericity are presented in Fig. 21(a) and (b), respectively. The pore size distribution exhibits a peak at approximately 2 mm, which is around 70 % of the peak size of the cells. This indicates that the majority of the pores are relatively large in comparison to the cells they reside in, pointing to a loosely packed structure in the packing. Similarly, the distribution of pore sphericity mirrors the trend observed in cell sphericity, with a peak near 0.65, slightly exceeding the peak of cell sphericity. The presence of a long tail at lower sphericity values suggests that distorted pores frequently occur alongside distorted cells. The local void ratio is characterized by the porosity of a pore, which is defined as the ratio between pore volume and Delaunay cell volume. Fig. 21(c) gives the distribution of pore porosity within the packing. The distribution exhibits a plateau ranging from 0.32 to 0.47, indicating the non-uniformity and irregularity of the pore structures. Additionally, it can be observed that the distribution gradually decreases towards 0 as porosity approaches 1. This indicates the presence of a small number of distorted pores, where the particles within a cell are positioned far apart, resulting in a porosity close to 1. Similarly, Fig. 21(d) illustrates the correlation between pore size and porosity. While it is generally more likely for larger pore to have a larger void ratio, there is a considerable number of small cells that exhibit relatively high void ratios, which should be related to small particles near a pore structure.

The results further reveal the complex internal structure of the packing. Due to the combined effects of liquid-induced cohesive forces and the multi-sized distribution of particles, various shapes of void spaces emerge, influenced by packing features such as agglomerates and chain-like particles. As a result, the packing exhibits a complicated pore structure. In fact, as mentioned above, all the analysis in this study just presents some quantitative results of a complicated packing of multi-sized particles under strong cohesive forces, as qualitatively depicted in Figs. 3 and 4.

4. Conclusion

A detailed experimental analysis of the packing structure of multi-sized spheres with liquid addition has been studied, revealing intricate microstructural characteristics influenced by the capillary and inter-particle forces. Utilizing analytical techniques such as CN analysis, PCF analysis, the Voronoi and Delaunay tessellation, key features such as agglomerates, particle chains, and heterogeneous clusters of particles in both contact and non-contact states are identified and quantified. The following conclusions can be drawn from the present study:

1) Liquid addition significantly impacts the packing structure, resulting in higher porosity compared to dry conditions. CN analysis revealed that larger particles tend to have higher mean CN values, while smaller particles frequently form clusters around larger particles, enhancing overall connectivity within the packing. PCF analysis further corroborated these findings, showing prominent peaks corresponding to average distances between different particle types and highlighting the complex interplay between particle size and liquid content or cohesive force.
2) Voronoi tessellation revealed that the topological properties such as polyhedral faces and cell structures are significantly influenced by

particle size, with larger particles typically surrounded by numerous smaller particles. The metric properties of the Voronoi cells, such as face perimeter, area, and volume, provide insights into the spatial arrangement and connectivity of particles, emphasizing the role of capillary forces in shaping the packing structure.

3) Delaunay tessellation offered a complementary perspective, focusing on tetrahedral subunits and pore structures. The correlation between Delaunay cell size and sphericity indicated a trend towards more regular, near-spherical shapes for larger cells. The pore size distribution suggested a loosely packed structure with substantial void spaces. The analysis of pore porosity highlighted the non-uniformity and irregularity of the pore structures, as well as the complexity introduced by the multi-sized particle distribution and liquid-induced cohesive forces.

This study enhances our understanding of the packing dynamics of multi-sized wet spheres, providing valuable insights for the development of improved simulation methods that consider capillary and other liquid-related forces. The data are useful for testing the applicability of computer simulation when applied to liquid-related cohesive particles. They are available to interested researchers.

CRediT authorship contribution statement

Yi Zou: Writing – review & editing, Writing – original draft. **Junqi Xu:** Methodology. **Yongli Wu:** Writing – review & editing. **Ruiping Zou:** Writing – review & editing, Methodology. **Aibing Yu:** Supervision.

Declaration of competing interest

The authors declare that they have no known competing financial interests or personal relationships that could have appeared to influence the work reported in this paper.

Acknowledgements

The authors are grateful to the financial support from the National Natural Science Foundation of China (No. 52034003 & No. 52006035) and the Natural Science Foundation of Jiangsu Province (No. BK20200269), the ARC Research Hub for Smart Process Design and Control IH230100010 and the Australia NCI Supercomputing Facility.

Data availability

Data will be made available on request.

References

[1] R.M. German, Particle Packing Characteristics, Metal Powder Industries Federation, 1989.
[2] K.E. Thompson, H.S. Fogler, Modeling flow in disordered packed beds from pore-scale fluid mechanics, AIChE J 43 (1997) 1377–1389, https://doi.org/10.1002/aic.690430602.
[3] G.J. Cheng, A.B. Yu, P. Zulli, Evaluation of effective thermal conductivity from the structure of a packed bed, Chem. Eng. Sci. 54 (1999) 4199–4209, https://doi.org/10.1016/S0009-2509(99)00125-6.
[4] A.J. Sederman, P. Alexander, L.F. Gladden, Structure of packed beds probed by magnetic resonance imaging, Powder Technol. 117 (2001) 255–269, https://doi.org/10.1016/S0032-5910(00)00374-0.
[5] T. Aste, M. Saadatfar, T.J. Senden, Geometrical structure of disordered sphere packings, Phys. Rev. E 71 (2005) 061302, https://doi.org/10.1103/PhysRevE.71.061302.
[6] R. Moreno-Atanasio, R.A. Williams, X. Jia, Combining X-ray microtomography with computer simulation for analysis of granular and porous materials, Particuology 8 (2010) 81–99, https://doi.org/10.1016/j.partic.2010.01.001.
[7] L.F. Liu, Z.P. Zhang, A.B. Yu, Dynamic simulation of the centripetal packing of mono-sized spheres, Physica A 268 (1999) 433–453, https://doi.org/10.1016/S0378-4371(99)00106-5.
[8] R.Y. Yang, R.P. Zou, A.B. Yu, Computer simulation of the packing of fine particles, Phys. Rev. E 62 (2000) 3900–3908, https://doi.org/10.1103/PhysRevE.62.3900.
[9] R.Y. Yang, R.P. Zou, A.B. Yu, Numerical study of the packing of wet coarse uniform spheres, AICHE J. 49 (2003) 1656–1666, https://doi.org/10.1002/aic.690490706.
[10] P.A. Cundall, O.D. Strack, A discrete numerical model for granular assemblies, Geotechnique 29 (1979) 47–65.
[11] J.D. Bernal, J. Mason, Packing of spheres: co-ordination of randomly packed spheres, Nature 188 (1960) 910–911, https://doi.org/10.1038/188910a0.
[12] G.D. Scott, Packing of spheres: packing of equal spheres, Nature 188 (1960) 908–909, https://doi.org/10.1038/188908a0.
[13] M. Oda, Co-ordination number and its relation to shear strength of granular material, Soils Found. 17 (1977) 29–42, https://doi.org/10.3208/sandf1972.17.2_29.
[14] N. Ouchiyama, T. Tanaka, Porosity estimation for random packings of spherical particles, Ind. Eng. Chem. Fundam. 23 (1984) 490–493, https://doi.org/10.1021/i100016a019.
[15] J.S. Goodling, M.S. Khader, Co-ordination number distribution of spherical particles in a packed cylindrical bed, Powder Technol. 44 (1985) 53–55, https://doi.org/10.1016/0032-5910(85)85020-8.
[16] D. Pinson, R.P. Zou, A.B. Yu, P. Zulli, M.J. McCarthy, Coordination number of binary mixtures of spheres, J. Phys. D. Appl. Phys. 31 (1998) 457, https://doi.org/10.1088/0022-3727/31/4/016.
[17] R.P. Zou, X. Bian, D. Pinson, R.Y. Yang, A.B. Yu, P. Zulli, Coordination number of ternary mixtures of spheres†, Part. Part. Syst. Charact. 20 (2003) 335–341, https://doi.org/10.1002/ppsc.200390040.
[18] T. Aste, M. Saadatfar, T.J. Senden, Local and global relations between the number of contacts and density in monodisperse sphere packs, J. Stat. Mech. 2006 (2006) P07010, https://doi.org/10.1088/1742-5468/2006/07/P07010.
[19] J.A. Dodds, The porosity and contact points in multicomponent random sphere packings calculated by a simple statistical geometric model, J. Colloid Interface Sci. 77 (1980) 317–327, https://doi.org/10.1016/0021-9797(80)90302-1.
[20] M. Okazaki, T. Yamasaki, S. Gotoh, R. Toei, Eeefective thermal conductivity for granular beds of various binary mixtures, J. Chem. Eng. Jpn 14 (1981) 183–189.
[21] N. Ouchiyama, T. Tanaka, Porosity of a mass of solid particles having a range of sizes, Ind. Eng. Chem. Fundam. 20 (1981) 66–71, https://doi.org/10.1021/i100001a013.
[22] M. Suzuki, T. Oshima, Co-ordination number of a multi-component randomly packed bed of spheres with size distribution, Powder Technol. 44 (1985) 213–218, https://doi.org/10.1016/0032-5910(85)85002-6.
[23] E.M. Tory, N.A. Cochrane, S.R. Waddell, Anisotropy in simulated random packing of equal spheres, Nature 220 (1968) 1023–1024, https://doi.org/10.1038/2201023a0.
[24] J.L. Finney, Fine structure in randomly packed, dense clusters of hard spheres, Mater. Sci. Eng. 23 (1976) 199–205, https://doi.org/10.1016/0025-5416(76)90194-4.
[25] M.J. Powell, Computer-simulated random packing of spheres, Powder Technol. 25 (1980) 45–52, https://doi.org/10.1016/0032-5910(80)87007-0.
[26] L. Oger, J.P. Troadec, D. Bideau, J.A. Dodds, M.J. Powell, Properties of disordered sphere packings I. Geometric structure: statistical model, numerical simulations and experimental results, Powder Technol. 46 (1986) 121–131, https://doi.org/10.1016/0032-5910(86)80018-3.
[27] G.T. Nolan, P.E. Kavanagh, Computer simulation of random packing of hard spheres, Powder Technol. 72 (1992) 149–155, https://doi.org/10.1016/0032-5910(92)88021-9.
[28] A.S. Clarke, H. Jónsson, Structural changes accompanying densification of random hard-sphere packings, Phys. Rev. E 47 (1993) 3975–3984, https://doi.org/10.1103/PhysRevE.47.3975.
[29] Z.P. Zhang, L.F. Liu, Y.D. Yuan, A.B. Yu, A simulation study of the effects of dynamic variables on the packing of spheres, Powder Technol. 116 (2001) 23–32, https://doi.org/10.1016/S0032-5910(00)00356-9.
[30] C.H. Bennett, Serially deposited amorphous aggregates of hard spheres, J. Appl. Phys. 43 (2003) 2727–2734, https://doi.org/10.1063/1.1661585.
[31] R.Y. Yang, R.P. Zou, A.B. Yu, Effect of material properties on the packing of fine particles, J. Appl. Phys. 94 (2003) 3025–3034, https://doi.org/10.1063/1.1598638.
[32] R.Y. Yang, R.P. Zou, K.J. Dong, X.Z. An, A. Yu, Simulation of the packing of cohesive particles, Comput. Phys. Commun. 177 (2007) 206–209, https://doi.org/10.1016/j.cpc.2007.02.043.
[33] L. Oger, A. Gervois, J.P. Troadec, N. Rivier, Voronoi tessellation of packings of spheres: topological correlation and statistics, Philos. Mag. B 74 (1996) 177–197, https://doi.org/10.1080/01418639608240335.
[34] R.Y. Yang, R.P. Zou, A.B. Yu, Voronoi tessellation of the packing of fine uniform spheres, Phys. Rev. E 65 (2002) 041302, https://doi.org/10.1103/PhysRevE.65.041302.
[35] L.Y. Yi, K.J. Dong, R.P. Zou, A.B. Yu, Radical tessellation of the packing of ternary mixtures of spheres, Powder Technol. 224 (2012) 129–137, https://doi.org/10.1016/j.powtec.2012.02.042.
[36] L.Y. Yi, K.J. Dong, R.P. Zou, A.B. Yu, Radical tessellation of the packing of spheres with a log-normal size distribution, Phys. Rev. E 92 (2015) 032201, https://doi.org/10.1103/PhysRevE.92.032201.
[37] A.B. Yu, C.L. Feng, R.P. Zou, R.Y. Yang, On the relationship between porosity and interparticle forces, Powder Technol. 130 (2003) 70–76, https://doi.org/10.1016/S0032-5910(02)00228-0.
[38] J. Blum, R. Schräpler, Structure and mechanical properties of high-porosity macroscopic agglomerates formed by random ballistic deposition, Phys. Rev. Lett. 93 (2004) 115503, https://doi.org/10.1103/PhysRevLett.93.115503.
[39] D. Lohse, R. Rauhé, R. Bergmann, D. van der Meer, Creating a dry variety of quicksand, Nature 432 (2004) 689–690, https://doi.org/10.1038/432689a.

[40] K.J. Dong, R.Y. Yang, R.P. Zou, A.B. Yu, Role of Interparticle forces in the formation of random loose packing, Phys. Rev. Lett. 96 (2006) 145505, https://doi.org/10.1103/PhysRevLett.96.145505.
[41] P.B. Umbanhowar, D.I. Goldman, Low density fragile states in cohesive powders, Am. J. Phys. 74 (2006) 720–721, https://doi.org/10.1119/1.2201858.
[42] E.J.R. Parteli, J. Schmidt, C. Blümel, K.-E. Wirth, W. Peukert, T. Pöschel, Attractive particle interaction forces and packing density of fine glass powders, Sci. Rep. 4 (2014) 6227, https://doi.org/10.1038/srep06227.
[43] S. Herminghaus, Dynamics of wet granular matter, Adv. Phys. 54 (2005) 221–261, https://doi.org/10.1080/00018730500167855.
[44] Y.I. Rabinovich, M.S. Esayanur, B.M. Moudgil, Capillary forces between two spheres with a fixed volume liquid bridge: theory and experiment, Langmuir 21 (2005) 10992–10997, https://doi.org/10.1021/la0517639.
[45] M. Scheel, R. Seemann, M. Brinkmann, M. Di Michiel, A. Sheppard, B. Breidenbach, S. Herminghaus, Morphological clues to wet granular pile stability, Nat. Mater. 7 (2008) 189–193, https://doi.org/10.1038/nmat2117.
[46] M. Scheel, R. Seemann, M. Brinkmann, M. Di Michiel, A. Sheppard, S. Herminghaus, Liquid distribution and cohesion in wet granular assemblies beyond the capillary bridge regime, J. Phys. Condens. Matter 20 (2008) 494236, https://doi.org/10.1088/0953-8984/20/49/494236.
[47] H.-J. Butt, M. Kappl, Normal capillary forces, Adv. Colloid Interf. Sci. 146 (2009) 48–60, https://doi.org/10.1016/j.cis.2008.10.002.
[48] C.L. Feng, A.D. Yu, Effect of liquid addition on the packing of mono-sized coarse spheres, Powder Technol. 99 (1998) 22–28, https://doi.org/10.1016/S0032-5910(98)00086-2.
[49] R.-P. Zou, C.-L. Feng, A.-B. Yu, Packing density of binary mixtures of wet spheres, J. Am. Ceram. Soc. 84 (2001) 504–508, https://doi.org/10.1111/j.1151-2916.2001.tb00690.x.
[50] R.P. Zou, J.Q. Xu, C.L. Feng, A.B. Yu, S. Johnston, N. Standish, Packing of multi-sized mixtures of wet coarse spheres, Powder Technol. 130 (2003) 77–83, https://doi.org/10.1016/S0032-5910(02)00229-2.
[51] J.Q. Xu, R.P. Zou, A.B. Yu, Packing structure of cohesive spheres, Phys. Rev. E 69 (2004) 032301, https://doi.org/10.1103/PhysRevE.69.032301.
[52] J.Q. Xu, R.P. Zou, A.B. Yu, Analysis of the packing structure of wet spheres by Voronoi–Delaunay tessellation, Granul. Matter 9 (2007) 455–463, https://doi.org/10.1007/s10035-007-0052-4.
[53] Z. Wang, J.-M. Pereira, Y. Gan, Packing of wet monodisperse spheres, Powder Technol. 378 (2021) 60–64, https://doi.org/10.1016/j.powtec.2020.09.074.
[54] O.B. Kovalev, I.O. Kovaleva, Modeling of the random packing of a loose layer of polydisperse spherical particles, J. Appl. Mech. Tech. Phys. 55 (2014) 709–717, https://doi.org/10.1134/S0021894414040178.
[55] W. Liu, S. Li, S. Chen, Computer simulation of random loose packings of micro-particles in presence of adhesion and friction, Powder Technol. 302 (2016) 414–422, https://doi.org/10.1016/j.powtec.2016.08.068.
[56] H. Chen, W. Liu, S. Li, Random loose packing of small particles with liquid cohesion, AIChE J 65 (2019) 500–511, https://doi.org/10.1002/aic.16440.
[57] W. Liu, S. Chen, S. Li, Random loose packings of polydisperse adhesive microparticles with Gaussian size distribution, Powder Technol. 357 (2019) 64–73, https://doi.org/10.1016/j.powtec.2019.08.092.
[58] K.L. Johnson, K. Kendall, A.D. Roberts, D. Tabor, Surface energy and the contact of elastic solids, Proc. R. Soc. Lond. A Math. Phys. Sci. 324 (1997) 301–313, https://doi.org/10.1098/rspa.1971.0141.
[59] N. Mitarai, F. Nori, Wet granular materials, Adv. Phys. 55 (2006) 1–45, https://doi.org/10.1080/00018730600626065.
[60] M. Dong, Z. Wang, Y. Gan, Wet mono-sized granular packing: effects of initial clusters and filling strategy, Powder Technol. 407 (2022) 117678, https://doi.org/10.1016/j.powtec.2022.117678.
[61] L.Y. Yi, K.J. Dong, R.P. Zou, A.B. Yu, Coordination number of the packing of ternary mixtures of spheres: DEM simulations versus measurements, Ind. Eng. Chem. Res. 50 (2011) 8773–8785, https://doi.org/10.1021/ie200765h.
[62] C.H. Rycroft, VORO++: a three-dimensional Voronoi cell library in C++, Chaos: an interdisciplinary, J. Nonlinear Sci. 19 (2009), https://doi.org/10.1063/1.3215722.
[63] G.J. Cheng, A.B. Yu, Evaluation of effective thermal conductivity from the structure of a packed bed: radiation heat transfer, Ind. Eng. Chem. Res. 52 (34) (2013) 12202–12211.
[64] Y. Wu, Q. Hou, A. Yu, Pore-scale study of fluid flow and drag force in randomly packed beds of different porosities, Ind. Eng. Chem. Res. 58 (2019) 5041–5053, https://doi.org/10.1021/acs.iecr.8b06418.
[65] Y. Wu, Q. Hou, Z. Qi, A. Yu, Particle–pore scale modelling of particle–fluid flows, Chem. Eng. Sci. 235 (2021), https://doi.org/10.1016/j.ces.2021.116500.